Research article JHEP|Reports

Imaging features of histological subtypes of hepatocellular carcinoma: Implication for LI-RADS

Authors

Roberto Cannella, Marco Dioguardi Burgio, Aurélie Beaufrère, Loïc Trapani, Valérie Paradis, Christian Hobeika, Francois Cauchy, Mohamed Bouattour, Valérie Vilgrain, Riccardo Sartoris, Maxime Ronot

Correspondence

marco_dioguardi@hotmail.it (M. Dioguardi Burgio).

Graphical abstract

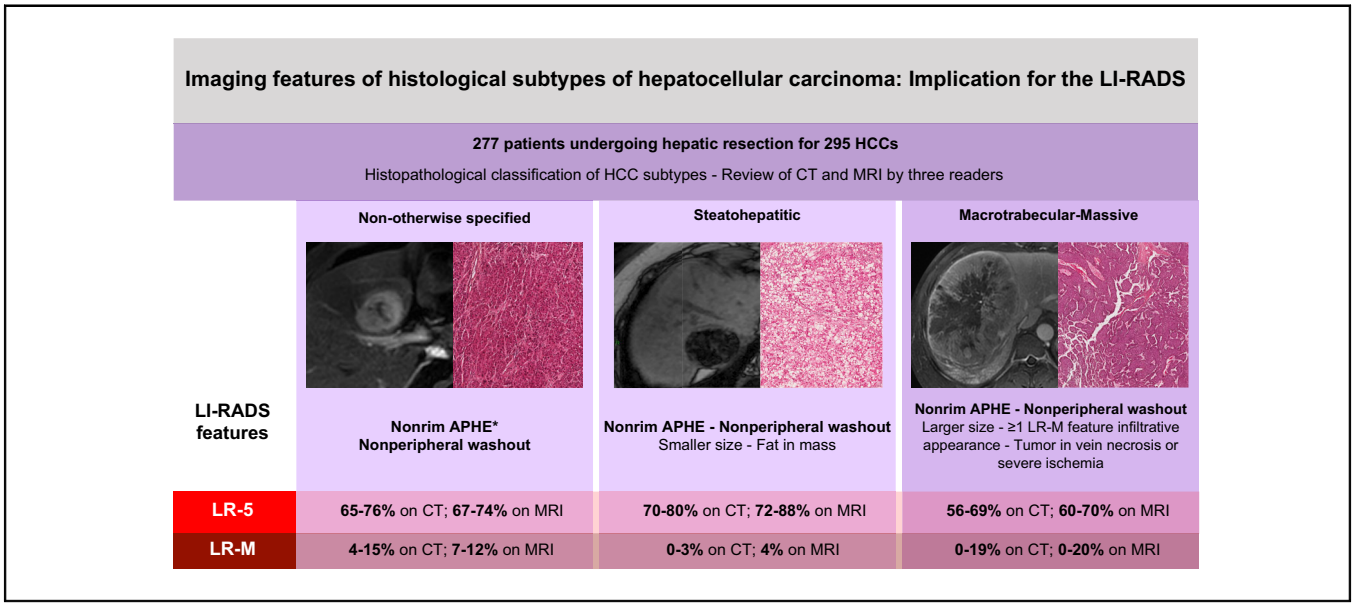

Highlights

- The distribution of the major features and categories of LI-RADS is not different among the HCC histological subtypes.
- MTM-HCC was associated with TIV, ≥1 LR-M feature, infiltrative appearance, necrosis or severe ischaemia, and larger size.
- Steatohepatitis-related HCC was associated with fat in mass on CT and on MRI.

Lay summary

In high-risk patients, the overall distribution of LI-RADS major features and categories is not different among the histological subtypes of hepatocellular carcinoma, but tumour-in-vein, presence of LR-M features, and ancillary features can provide information for the non-invasive diagnosis of hepatocellular carcinoma subtypes.

https://doi.org/10.1016/j.jhepr.2021.100380

Research article

JHEP|Reports

Imaging features of histological subtypes of hepatocellular carcinoma: Implication for LI-RADS

Roberto Cannella,[1,2,3,†] Marco Dioguardi Burgio,[1,4,†,*] Aurélie Beaufrère,[5] Loïc Trapani,[5] Valérie Paradis,[5] Christian Hobeika,[6] Francois Cauchy,[6] Mohamed Bouattour,[7] Valérie Vilgrain,[1,4] Riccardo Sartoris,[1,4] Maxime Ronot[1,4]

[1]*Department of Radiology, Hôpital Beaujon, Clichy, France;* [2]*Section of Radiology–BiND, University Hospital 'Paolo Giaccone', Palermo, Italy;* [3]*Department of Health Promotion Sciences Maternal and Infant Care, Internal Medicine and Medical Specialties, PROMISE, University of Palermo, Palermo, Italy;* [4]*Université de Paris, INSERM U1149 'centre de recherche sur l'inflammation', CRI, Paris, France;* [5]*Department of Pathology, Hôpital Beaujon, Clichy, France;* [6]*Department of HPB Surgery and Liver Transplantation, Hôpital Beaujon, Clichy, France;* [7]*Department of Digestive Oncology, Hôpital Beaujon, Clichy, France*

JHEP Reports **2021.** https://doi.org/10.1016/j.jhepr.2021.100380

Background & Aims: The histopathological subtypes of hepatocellular carcinoma (HCC) are associated with distinct clinical features and prognoses. This study aims to report Liver Imaging Reporting and Data System (LI-RADS)-defined imaging features of different HCC subtypes in a cohort of resected tumours and to assess the influence of HCC subtypes on computed tomography (CT)/magnetic resonance imaging (MRI) LI-RADS categorisation in the subgroup of high-risk patients.
Methods: This retrospective institutional review board-approved study included patients with resected HCCs and available histopathological classification. Three radiologists independently reviewed preoperative CT and MRI exams. The readers evaluated the presence of imaging features according to LI-RADS v2018 definitions and provided a LI-RADS category in patients at high risk of HCC. Differences in LI-RADS features and categorisations were assessed for not otherwise specified (NOS-HCC), steatohepatitic (SH-HCC), and macrotrabecular-massive (MTM-HCC) types of HCCs.
Results: Two hundred and seventy-seven patients (median age 64.0 years, 215 [77.6%] men) were analysed, which involved 295 HCCs. There were 197 (66.7%) NOS-HCCs, 62 (21.0%) SH-HCCs, 23 (7.8%) MTM-HCCs, and 13 (4.5%) other rare subtypes. The following features were more frequent in MTM-HCC: elevated α-foetoprotein serum levels (p <0.001), tumour-in-vein (p <0.001 on CT, p ≤0.052 on MRI), presence of at least 1 LR-M feature (p ≤0.010 on CT), infiltrative appearance (p ≤0.032 on CT), necrosis or severe ischaemia (p ≤0.038 on CT), and larger size (p ≤0.006 on CT, p ≤0.011 on MRI). SH-HCC was associated with fat in mass (p <0.001 on CT, p ≤0.002 on MRI). The distribution of the LI-RADS major features and categories in high-risk patients did not significantly differ among the 3 main HCC subtypes.
Conclusions: The distribution of LI-RADS major features and categories is not different among the HCC subtypes. Nevertheless, careful analysis of tumour-in-vein, LR-M, and ancillary features as well as clinico-biological data can provide information for the non-invasive diagnosis of HCC subtypes.
Lay summary: In high-risk patients, the overall distribution of LI-RADS major features and categories is not different among the histological subtypes of hepatocellular carcinoma, but tumour-in-vein, presence of LR-M features, and ancillary features can provide information for the non-invasive diagnosis of hepatocellular carcinoma subtypes.

Introduction

Hepatocellular carcinoma (HCC) is the leading cause of cancer-related mortality in patients with chronic liver disease. Among other things, the prognosis of patients with HCC is affected by the biological aggressiveness of the tumour. Although several histopathological features such as high tumour grade, the presence of satellite nodules, macrovascular and microvascular invasion have been associated with poorer outcomes,[1] others, such as the histological tumour subtype, are often overlooked.

The fifth edition of the World Health Organization (WHO) classification of conventional HCCs included not otherwise specified HCC (NOS-HCC) and around 35% of HCCs classified into 8 other specific subtypes based on histopathological architectural patterns and key molecular features.[2] Steatohepatitic HCC (SH-HCC) is the most common subtype (5–20% of HCCs), and it is associated with distinct molecular features, less aggressive histopathological phenotype, metabolic syndrome, and non-alcoholic fatty liver disease.[3–5] Macrotrabecular-massive HCC (MTM-HCC) represents 5–15% of all HCCs and is

Keywords: Hepatocellular carcinoma; LI-RADS; Histopathological subtypes; Computed tomography; Magnetic resonance imaging.
Received 3 August 2021; received in revised form 21 September 2021; accepted 22 September 2021; available online 30 September 2021
† These authors contributed equally to this work.
* Corresponding author. Address: Department of Radiology, Hôpital Beaujon, 100 boulevard du Général Leclerc, 92119 Clichy, France. Tel.: +33-140875566; Fax: +33-140870548.
E-mail address: marco_dioguardi@hotmail.it (M. Dioguardi Burgio).

the histopathological subtype associated with the poorest prognosis, greater metastatic spread, and vascular invasion.[6–9]

Pretreatment imaging plays a central role in clinical practice because biopsy is not required in high-risk patients with lesions showing typical imaging features of HCC. Nevertheless, non-invasive preoperative identification of HCC subtypes is anticipated to be crucial for patient management by providing additional information to adapt the treatment strategy. For instance, the MTM-HCC subtype has been reported to be an independent predictor of early and overall recurrence in patients after either surgical resection or radiofrequency ablation.[6] Only a few studies have described the imaging features of HCC subtypes, in particular MTM-HCC[10–16] and SH-HCC.[17] These studies have focused on a combination of subjectively defined qualitative imaging features on computed tomography (CT) and magnetic resonance imaging (MRI).

The Liver Imaging Reporting and Data System (LI-RADS) provides a standardised lexicon and stepwise algorithm to characterise liver observations in patients at high risk of HCC.[18] LI-RADS imaging features and categories have been shown to reliably stratify patient prognosis.[19,20] For instance, observations showing imaging features suggesting a non-HCC malignancy (the LR-M category) require a histopathological diagnosis and have been reported to be more aggressive histopathologically with a poorer prognosis[19,20] Data on the influence of HCC subtypes on the LI-RADS classification are scarce. A recent study by Mulé *et al.*[12] found that MTM-HCCs were less likely to be classified as LR-5 than were other HCC subtypes. This study included a relatively small number of lesions (n = 70, with 15 MTM-HCCs) from the high-risk population, and only a few LI-RADS imaging features were analysed in comparison with non-MTM-HCCs.[12] None of these prior studies have investigated the imaging features of SH-HCC in relation to LI-RADS.

The first aim of this study was to report on LI-RADS-defined imaging features in different HCC subtypes in a cohort of resected tumours. We also evaluated the influence of HCC subtypes on CT/MRI LI-RADS categorisation in the subgroup of high-risk patients.

Patients and methods

This retrospective observational study, together with a chart review, was approved by the local institutional review board (CRM-2105-153), and informed consent was waived because of the retrospective design.

Population

Our surgical and histopathological databases were queried to select adult patients that met the following inclusion criteria: (1) diagnosis of HCC after surgical resection performed between 2012 and 2019 at our institution (Hôpital Beaujon, Clichy, France); (2) available histopathological classification of HCC subtypes; and (3) preoperative contrast-enhanced CT or MRI within 3 months before surgery. Patients with combined hepatocellular-cholangiocarcinoma or with other combined tumours were ineligible for the study owing to the known different prognosis, clinical, and imaging features.[21] The initial population included 308 patients (median age 64.0 years [IQR 55.0–70.0 years], with 239 men and 69 women) who underwent HCC resection. Patients were excluded if they (1) had 3 or more resected HCCs to ensure a reliable pathological–radiological correlation in patients with multiple lesions in the same segment or lobe (n = 24); (2) underwent treatment before the CT or MRI exams (n = 5, including transarterial chemoembolisation in 3 and tumour ablation in 2); and (3) had HCC with massive bleeding, making imaging analysis of the underlying tumour impossible (n = 2) (Fig. 1).

The CT and MRI exams closest to the date of surgery were selected as index studies in patients who underwent multiple preoperative imaging studies. Patient-related variables were collected, including demographic data, the aetiology of chronic liver disease, the history of HCC, the presence of cirrhosis, laboratory markers, recurrence-free survival (RFS), and overall survival (OS). RFS was measured from the time of surgery to the time of death or the first postoperative recurrence, regardless of the site of recurrence. OS was measured from the time of surgery until the date of death or the last available postoperative follow-up.

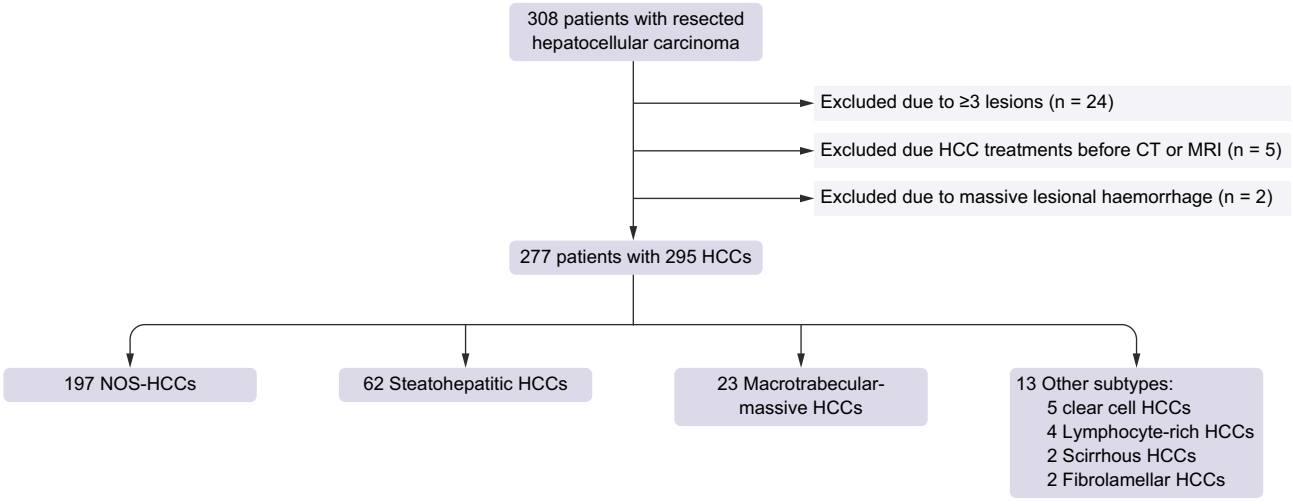

Fig. 1. Flowchart of the study population. CT, computed tomography; HCC, hepatocellular carcinoma; MRI, magnetic resonance imaging; NOS-HCC, not otherwise specified hepatocellular carcinoma.

Table 1. Clinical, laboratory, and histopathological characteristics of the patients with NOS-HCC, SH-HCC, and MTM-HCC subtypes.

Characteristics	All	NOS-HCC	SH-HCC	MTM-HCC	*p* value
Clinical and laboratory features					
Patients	266	186 (69.9)	59 (22.2)	21 (7.9)	–
Age (years)	64.0 (55.0, 70.0)	63.5 (55.0, 70.0)	66.0 (61.0, 70.0)	58.0 (43.5, 67.0)	**0.025**
Sex					0.187
Men	207 (77.8)	147 (79.0)	47 (79.7)	13 (61.9)	
Women	59 (22.2)	39 (21.0)	12 (20.3)	8 (38.1)	
Age men (years)	64.0 (55.0, 70.0)	62.0 (44.8, 70.0)	66.0 (62.0, 71.0)	53.0 (40.0, 68.0)	**0.026**
Age women (years)	66.0 (57.5, 70.0)	66.0 (59.0, 71.0)	66.5 (57.7, 68.7)	60.0 (45.7, 67.5)	0.409
Chronic liver disease*					
Hepatitis C	69 (25.9)	53 (28.5)	9 (15.3)	7 (33.3)	0.094
Hepatitis B	70 (26.3)	50 (26.9)	9 (15.3)	11 (52.4)	**0.004**
Alcohol abuse	48 (18.0)	29 (15.6)	18 (30.5)	1 (4.8)	**0.009**
NAFLD	90 (33.8)	52 (28.0)	32 (54.2)	6 (28.6)	**0.001**
Vascular liver disease	4 (1.5)	2 (1.1)	2 (3.4)	0 (0)	0.374
Others	13 (4.9)	9 (4.8)	4 (6.8)	0 (0)	0.464
No risk	32 (12.0)	22 (11.8)	7 (11.9)	3 (14.3)	0.947
Cirrhosis	85 (32.0)	55 (29.6)	24 (40.7)	6 (28.6)	0.264
LI-RADS high-risk status	141 (53.0)	96 (51.6)	30 (50.8)	15 (71.4)	0.211
AST (IU/L)	45.0 (33.0, 73.0)	45.0 (31.2, 72.0)	41.0 (33.0, 57.5)	100.0 (56.7, 162.7)	**<0.001**
ALT (IU/L)	43.0 (28.0, 69.0)	43.5 (26.2, 69.0)	39.0 (26.7, 53.0)	67.0 (42.0, 117.2)	**0.006**
Albumin (g/L)	38.0 (34.0, 41.0)	38.0 (35.0, 41.0)	38.5 (34.0, 43.0)	35.0 (27.0, 39.2)	**0.023**
Creatinine (μmol/L)	80.0 (70.0, 95.0)	78.0 (69.0, 95.0)	86.0 (74.5, 98.0)	79.0, (66.2, 84.5)	0.061
Total bilirubin (mg/L)	10.0 (7.0, 14.0)	9.0 (7.0, 14.0)	8.0 (7.0, 11.5)	12.0 (8.7, 15.5)	0.504
Platelet count ($\times 10^3/\mu l$)	209 (157, 248)	209 (160, 246)	200 (142, 248)	230 (198, 314)	0.435
α-foetoprotein (ng/ml)	9.0 (4.0, 183.0)	8.0 (4.0, 124.0)	6.0 (3.0, 32.0)	14700 (111, 27650)	**<0.001**
RFS (median, 95% CI)	39.0 (26.7, 51.3)	38.0 (25.6, 50.4)	58.0 (29.4, 86.6)	18.0 (1.0, 39.1)	0.698
OS (median, 95% CI)	88.0 (69.8, 104.3)	Not reached	82.0 (69.8, 94.1)	65.0 (46.4, 76.7)	0.750
Histopathological features					
HCC	282	197 (69.9)	62 (22.0)	23 (8.1)	–
Edmonson–Steiner grade					**0.004**
I–II	84 (29.8)	66 (33.5)	18 (29.0)	0 (0)	
III–IV	198 (70.2)	131 (66.5)	44 (71.0)	23 (100)	
Macrovascular invasion	30 (10.6)	16 (8.1)	3 (4.8)	11 (47.8)	**<0.001**
Microvascular invasion	162 (57.4)	116 (58.9)	26 (41.9)	20 (87.0)	**0.001**
Satellite nodules	60 (21.3)	39 (19.8)	11 (17.7)	10 (43.5)	**0.024**
Macroscopic capsule	193 (68.4)	147 (74.6)	33 (53.2)	13 (56.5)	**0.003**
Microscopic capsule	211 (74.8)	153 (77.7)	42 (67.7)	16 (69.6)	0.243
Hepatic steatosis					**0.008**
None	171 (60.0)	128 (65.0)	25 (40.3)	18 (78.3)	
Mild	78 (27.7)	47 (23.9)	28 (45.2)	3 (13.0)	
Moderate	31 (11.0)	20 (10.2)	9 (14.5)	2 (8.7)	
Severe	2 (0.7)	2 (1.0)	0 (0)	0 (0)	
Hepatic fibrosis stage					0.845
F0	31 (11.0)	23 (11.7)	4 (6.5)	4 (17.4)	
F1	42 (14.9)	30 (15.2)	9 (14.4)	3 (13.0)	
F2	54 (19.1)	40 (20.3)	11 (17.7)	3 (13.0)	
F3	65 (23.1)	45 (22.8)	14 (22.6)	6 (26.1)	
F4	90 (31.9)	59 (29.9)	24 (38.7)	7 (30.4)	

Continuous variables are expressed as medians and IQRs (25th to 75th percentiles) in parentheses, and categorical variables are expressed as numbers and percentages in parentheses. Continuous variables were compared using the Kruskal-Wallis test. Categorial variables were compared using the the Pearson $\chi 2$ test. Statistically significant values (p <0.05) are highlighted in bold. In patients with 2 HCCs, the largest lesion was considered for subclassification.

ALT, alanine transaminase; AST, aspartate transaminase; HCC, hepatocellular carcinoma; LI-RADS, Liver Imaging Reporting and Data System; MTM-HCC, macrotrabecular massive hepatocellular carcinoma; NAFLD, non-alcoholic fatty liver disease; NOS-HCC, not otherwise specified hepatocellular carcinoma; OS, overall survival; RFS, recurrence-free survival; SH-HCC, steatohepatitic hepatocellular carcinoma.

* More than 1 aetiology could be present in each patient.

Imaging technique

Patients underwent multiphase contrast-enhanced CT and/or MRI with liver protocols acquired in accordance with LI-RADS technical recommendations.[22] Details of the imaging protocols are reported in the Supplementary information. The median time between the index CT and MRI exams and surgical resection was 34 days (IQR 15–53 days) and 41 days (IQR 23–63 days), respectively. Overall, 262/295 (88.8%) HCCs were examined on contrast-enhanced CT (including 137 observations in high-risk patients), whereas MRI was available in 237/295 (80.3%) HCCs (127 in high-risk patients).

Imaging analysis

Three radiologists (R1 [MDB], R2 [RS], and R3 [RC], with 10, 8, and 6 years of experience in abdominal and liver imaging, respectively) independently reviewed all the imaging exams. Readers were aware of the diagnosis of HCC but blinded to the histopathological analysis. The readers evaluated the presence of imaging features on CT and MRI exams based on the LI-RADS v2018 definitions.[18] CT and MRI exams were reviewed independently and in random order to minimise recall bias. Imaging features included tumour-in-vein (TIV), LR-M features (both targetoid and non-targetoid features), major features (size, non-rim arterial phase hyperenhancement [APHE], non-peripheral 'washout',

Table 2. Differences in LI-RADS-defined TIV, LR-M, and major features in NOS-HCC, SH-HCC, and MTM-HCC subtypes in the entire cohort with contrast-enhanced CT (n = 253).

Features	NOS-HCC (n = 175)	SH-HCC (n = 58)	MTM-HCC (n = 20)	*p* value	R1 *vs.* R2 N agreement (%) κ value (95% CI)	R1 *vs.* R3 N agreement (%) κ value (95% CI)	R2 *vs.* R3 N agreement (%) κ value (95% CI)
TIV							
R1	9 (5.1)	1 (1.7)	6 (30.0)	**<0.001**	240 (94.8)	246 (97.2)	241 (95.2)
R2	16 (9.1)	2 (3.4)	7 (35.0)	**<0.001**	0.65 (0.48, 0.82)	0.74 (0.56, 0.92)	0.61 (0.48, 0.83)
R3	7 (4.0)	1 (1.7)	5 (25.0)	**<0.001**			
LR-M features							
At least 1 LR-M feature							
R1	76 (43.4)	13 (22.4)	13 (65.0)	**0.001**	208 (82.2)	214 (84.6)	209 (82.6)
R2	76 (43.4)	13 (22.4)	10 (50.0)	**0.010**	0.62 (0.53, 0.72)	0.66 (0.57, 0.76)	0.62 (0.52, 0.72)
R3	59 (33.7)	7 (12.1)	11 (55.0)	**<0.001**			
At least 1 targetoid feature							
R1	12 (6.9)	1 (1.7)	3 (15.0)	0.096	233 (92.1)	241 (95.2)	233 (92.1)
R2	5 (2.9)	3 (5.2)	0 (0)	0.767	0.13 (−0.07, 0.33)	0.62 (0.42, 0.81)	0.19 (−0.02, 0.41)
R3	13 (7.4)	2 (3.4)	3 (15.0)	0.214			
Rim APHE							
R1	6 (3.4)	1 (1.7)	2 (10.0)	0.224	244 (96.5)	246 (97.3)	239 (94.5)
R2	2 (1.1)	2 (3.4)	0 (0)	0.399	0.29 (−0.03, 0.62)	0.70 (0.50, 0.91)	0.28 (0.02, 0.54)
R3	11 (6.3)	2 (3.4)	3 (15.0)	0.187			
Peripheral 'washout'							
R1	1 (0.6)	0 (0)	0 (0)	0.800	252 (99.6)	249 (98.4)	248 (98.0)
R2	0 (0)	0 (0)	0 (0)	1.000	0.00 (0.00, 0.00)	0.32 (−0.15, 0.81)	0.00 (0.00, 0.00)
R3	4 (2.3)	0 (0)	1 (5.0)	0.333			
Delayed central enhancement							
R1	3 (1.7)	0 (0)	1 (5.0)	0.293	245 (96.8)	246 (97.2)	246 (97.2)
R2	3 (1.7)	1 (1.7)	0 (0)	0.840	−0.01 (−0.02, −0.004)	−0.01 (−0.02, −0.003)	−0.01 (−0.02, −0.003)
R3	2 (1.1)	0 (0)	1 (5.0)	0.204			
Infiltrative appearance							
R1	16 (9.1)	2 (3.4)	5 (25.0)	**0.015**	241 (95.2)	239 (94.5)	239 (94.5)
R2	15 (8.6)	1 (1.7)	3 (15.0)	0.096	0.68 (0.52, 0.85)	0.60 (0.41, 0.79)	0.55 (0.35, 0.76)
R3	12 (6.9)	0 (0)	3 (15.0)	**0.032**			
Necrosis or severe ischaemia							
R1	55 (31.4)	11 (19.0)	9 (45.0)	0.058	217 (85.7)	220 (87.0)	214 (84.6)
R2	59 (33.7)	10 (17.2)	8 (40.0)	**0.038**	0.66 (0.56, 0.76)	0.66 (0.56, 0.77)	0.61 (0.50, 0.72)
R3	45 (25.7)	6 (10.3)	9 (45.0)	**0.004**			
Major features							
Size (mm)							
R1	42.0 (29.0, 71.0)	32.5 (20.0, 56.5)	94.0 (34.2, 137.5)	**0.002**	0.97 (0.96, 0.97)*	0.95 (0.94, 0.96)*	0.97 (0.96, 0.98)*
R2	48.0 (32.0, 80.0)	39.0 (23.0, 60.2)	104.0 (40.2, 139.5)	**0.003**			
R3	44.0 (27.0, 81.0)	36.0 (20.7, 60.0)	101.5 (32.2, 142.0)	**0.006**			
Non-rim APHE							
R1	155 (88.6)	53 (91.4)	16 (80.0)	0.387	231 (91.4)	230 (90.9)	216 (85.3)
R2	169 (96.6)	52 (89.7)	19 (95.0)	0.118	0.43 (0.24, 0.62)	0.65 (0.52, 0.68)	0.34 (0.19, 0.49)
R3	144 (82.3)	47 (81.0)	14 (70.0)	0.414			
Non-peripheral 'washout'							
R1	162 (92.6)	49 (84.5)	20 (100)	0.059	232 (91.7)	227 (89.7)	228 (86.1)
R2	161 (92.0)	50 (86.2)	19 (95.0)	0.331	0.48 (0.29, 0.67)	0.52 (0.37, 0.68)	0.37 (0.20, 0.53)
R3	148 (84.6)	48 (82.8)	17 (85.0)	0.943			
Enhancing 'capsule'							
R1	81 (46.3)	27 (46.6)	8 (40.0)	0.860	186 (73.5)	198 (78.3)	193 (76.3)
R2	108 (61.7)	32 (55.2)	13 (65.0)	0.617	0.47 (0.37, 0.58)	0.56 (0.46, 0.66)	0.53 (0.43, 0.63)
R3	81 (46.3)	31 (53.4)	7 (35.0)	0.340			
Threshold growth							
R1	7 (4.0)	3 (5.2)	2 (10.0)	0.482	245 (96.9)	243 (96.1)	245 (97.2)
R2	7 (4.0)	0 (0)	1 (5.0)	0.284	0.58 (0.32, 0.84)	0.48 (0.20, 0.75)	0.48 (0.17, 0.79)
R3	7 (4.0)	1 (1.7)	0 (0)	0.346			

Categorical variables are expressed as numbers and percentages in parentheses. The continuous variable (size) is reported as median and IQR (25th to 75th percentiles) in parentheses. Differences between HCC subtypes were assessed using the Pearson $\chi 2$ test for categorical variables. Inter-reader agreement was assessed using Cohen's kappa (κ) test for categorical variables and intraclass correlation coefficient of the continuous variable (size). Statistically significant values (p <0.05) are highlighted in bold.
APHE, arterial phase hyperenhancement; CT, computed tomography; HCC, hepatocellular carcinoma; LI-RADS, Liver Imaging Reporting and Data System; MTM-HCC, macrotrabecular massive hepatocellular carcinoma; NOS-HCC, not otherwise specified hepatocellular carcinoma; R1, Reader 1; R2, Reader 2; R3, Reader 3; SH-HCC, steatohepatitic hepatocellular carcinoma; TIV, tumour-in-vein.
* Agreement assessed with intraclass correlation coefficient.

enhancing 'capsule', and threshold growth), and ancillary features favouring malignancy (not HCC in particular and HCC in particular) and favouring benignity as defined in the LI-RADS v2018 core document. Ultrasound (US) visibility as a discrete nodule was not assessed because US imaging was only occasionally available in this cohort, whereas transitional phase hypointensity could not be assessed because of the lack of gadoxetate disodium and transitional phases. The presence of an adequate hepatobiliary phase

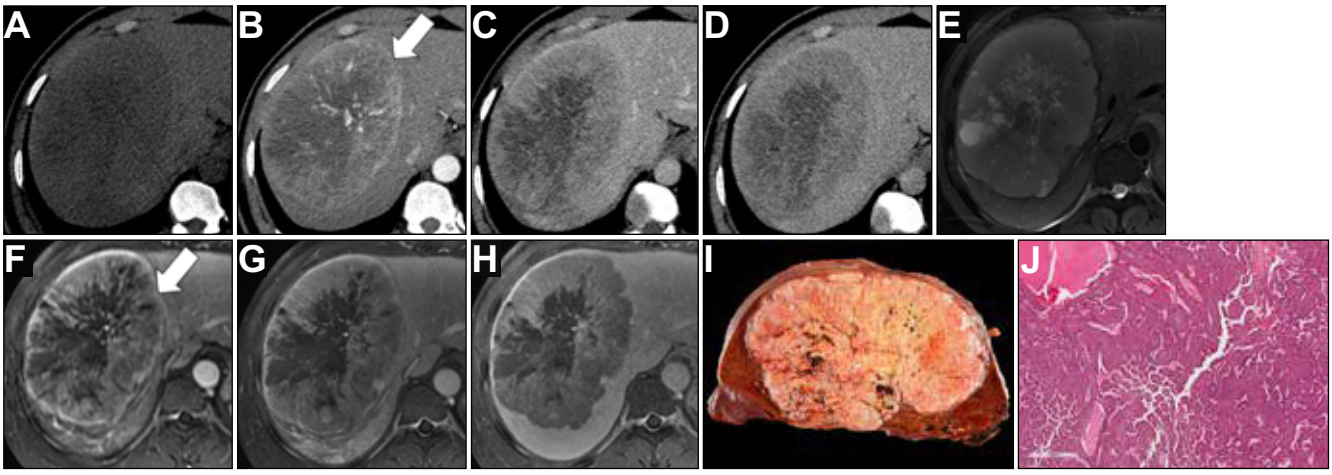

Fig. 2. A 32-year-old man with chronic hepatitis B infection and 151-mm macrotrabecular-massive hepatocellular carcinoma with CT (A–D) and MRI (E–H). The lesion showed non-rim arterial phase hyperenhancement (B and F, arrows), non-peripheral 'washout', and enhancing 'capsule' on portal venous phase and delayed phases (C–D and G–H). All readers were concordant with the presence of necrosis or severe ischaemia on both CT and MRI (A and E), and mild –moderate T2 hyperintensity on MRI (E). The observation was categorised as LR-5 by all readers on CT and MRI. Macroscopic examination of the resected specimen (I) showed well-demarcated encapsulated tumour with necrosis change. Microscopic examination (J) showed a macrotrabecular pattern with the area of necrosis consistent with the diagnosis of macrotrabecular-massive hepatocellular carcinoma. CT, computed tomography; MRI, magnetic resonance imaging.

(HBP), defined as a clearly hyperintense liver parenchyma in relation to the hepatic blood vessels,[18] was ensured before reviewing HBP-related imaging features.

As the LI-RADS categories can be applied only in high-risk patients (*i.e.* cirrhosis, HBV infection, or a history of or current HCC), the readers provided a LI-RADS category based on the major features only in the subset of patients considered to be at high risk of HCC according to the LI-RADS v2018 population criteria, and the final LI-RADS category was adjusted after considering ancillary features. Observations with non-targetoid LR-M features were categorised as LR-M in the absence of any LR-5 or LR-TIV features according to LI-RADS recommendation.[18]

Histopathological analysis

The haematein–eosin–safran slides of each tumour were reviewed by 2 pathologists (AB and LT). The following microscopic criteria were systematically assessed: differentiation (Edmonson–Steiner grade), architecture (microtrabecular,

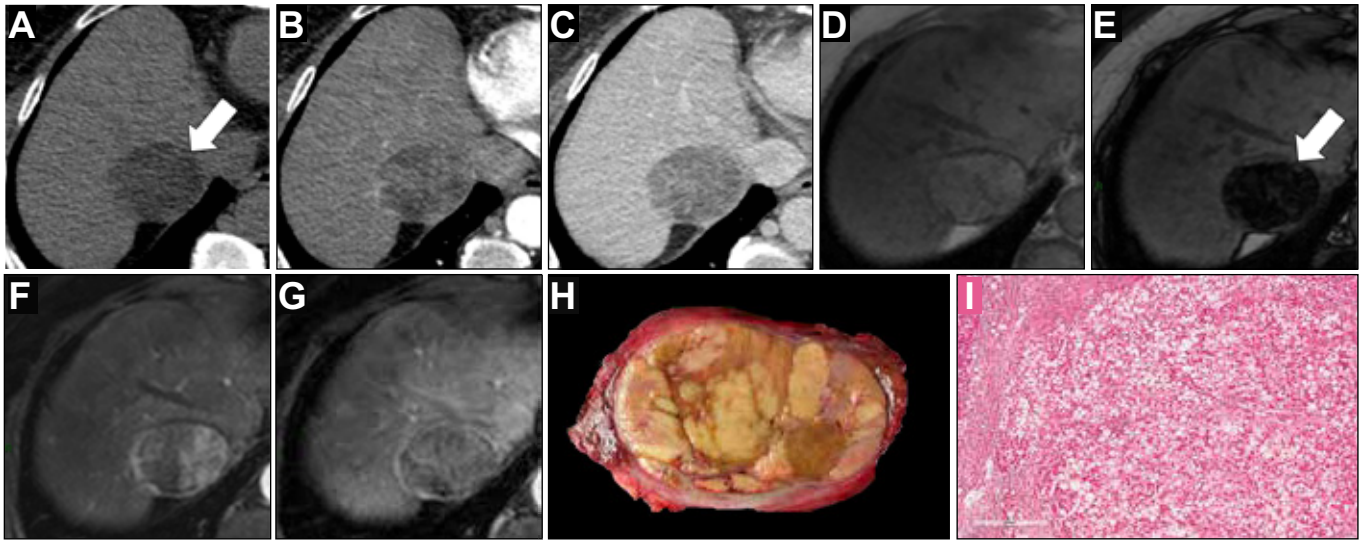

Fig. 3. A 60-year-old woman with hepatitis B-related cirrhosis and 51-mm steatohepatitic hepatocellular carcinoma with CT (A–C) and MRI (D–G). The lesion showed non-rim arterial phase hyperenhancement (B and F), non-peripheral 'washout', and enhancing 'capsule' on portal venous phases (C and G). All readers agreed on the presence of fat in mass as an ancillary feature, visible on pre-contrast CT image (A, arrow), and as marked signal drop on the MRI sequence (E, arrow). The observation was categorised as LR-5 by all readers on MRI and as LR-5 by 2 of 3 readers on CT. Macroscopic examination of the resected tumour (H) showed a well-demarcated encapsulated yellow tumour. Microscopic examination (I) showed a steatohepatitic pattern with numerous steatotic tumour cells and few ballooning tumour cells associated with fibrosis and lymphocytic inflammation consistent with the diagnosis of steatohepatitic hepatocellular carcinoma. CT, computed tomography; MRI, magnetic resonance imaging.

Table 3. LI-RADS categories using major features only and after final adjustment for ancillary features in NOS-HCC, SH-HCC, and MTM-HCC subtypes in high-risk patients with contrast-enhanced CT (n = 134).

	NOS-HCC (n = 88)	SH-HCC (n = 30)	MTM-HCC (n = 16)	*p* value
LI-RADS categories with major features only				
R1				0.063
LR-3	6 (6.8)	3 (10.0)	0 (0)	
LR-4	7 (8.0)	3 (10.0)	1 (6.2)	
LR-5	64 (72.7)	24 (80.0)	9 (56.2)	
LR-M	7 (8.0)	0 (0)	3 (18.8)	
LR-TIV	4 (4.5)	0 (0)	3 (18.8)	
R2				0.313
LR-3	2 (2.3)	3 (10.0)	1 (6.2)	
LR-4	5 (5.7)	2 (6.7)	0 (0)	
LR-5	67 (76.1)	23 (76.7)	11 (68.8)	
LR-M	4 (4.5)	1 (3.3)	0 (0)	
LR-TIV	10 (11.4)	1 (3.3)	4 (25.0)	
R3				0.172
LR-3	4 (4.5)	1 (3.3)	1 (6.2)	
LR-4	12 (13.6)	7 (23.3)	1 (6.2)	
LR-5	57 (64.8)	21 (70.0)	9 (56.2)	
LR-M	13 (14.8)	1 (3.3)	3 (18.8)	
LR-TIV	2 (2.3)	0 (0)	2 (12.5)	
Agreement	N agreement (%); κ value (95% CI)			
R1 *vs.* R2	105 (78.4); 0.48 (0.54, 0.62)			
R1 *vs.* R3	103 (76.9); 0.54 (0.40, 0.67)			
R2 *vs.* R3	96 (71.6): 0.42 (0.29, 0.55)			
LI-RADS categories with major and ancillary features				
R1				0.065
LR-3	5 (5.7)	2 (6.7)	0 (0)	
LR-4	8 (9.1)	4 (13.3)	1 (6.2)	
LR-5	64 (72.7)	24 (80.0)	9 (56.2)	
LR-M	7 (8.0)	0 (0)	3 (18.8)	
LR-TIV	4 (4.5)	0 (0)	3 (18.8)	
R2				0.386
LR-3	2 (2.3)	2 (6.7)	1 (6.2)	
LR-4	5 (5.7)	3 (10.0)	0 (0)	
LR-5	67 (76.1)	23 (76.7)	11 (68.8)	
LR-M	4 (4.5)	1 (3.3)	0 (0)	
LR-TIV	10 (11.4)	1 (3.3)	4 (25.0)	
R3				0.179
LR-3	3 (3.4)	1 (3.3)	1 (6.2)	
LR-4	13 (14.8)	7 (23.3)	1 (6.2)	
LR-5	57 (64.8)	21 (70.0)	9 (56.2)	
LR-M	13 (14.8)	1 (3.3)	3 (18.8)	
LR-TIV	2 (2.3)	0 (0)	2 (12.5)	
Agreement	N agreement (%); κ value (95% CI)			
R1 *vs.* R2	103 (76.9); 0.47 (0.33, 0.60)			
R1 *vs.* R3	102 (76.1); 0.55 (0.42, 0.68)			
R2 *vs.* R3	95 (70.9); 0.40 (0.28, 0.53)			

Differences between HCC subtypes were compared using the the Pearson $\chi 2$ test. Inter-reader agreement was assessed using Cohen's kappa (κ) test with 95% CI.
CT, computed tomography; LI-RADS, Liver Imaging Reporting and Data System; MTM-HCC, macrotrabecular massive hepatocellular carcinoma; NOS-HCC, not otherwise specified hepatocellular carcinoma; R1, Reader 1; R2, Reader 2; R3, Reader 3; SH-HCC, steatohepatitic hepatocellular carcinoma; TIV, tumour-in-vein.

macrotrabecular, pseudoglandular, and compact), capsule, vascular invasion, and satellite nodules.

HCCs were subdivided according to the WHO classification into NOS-HCC or HCC of specific variants[2]: steatohepatitic, clear cell, macrotrabecular-massive, scirrhous, chromophobe, fibrolamellar carcinoma, neutrophil-rich, and lymphocyte-rich.

The diagnosis of SH-HCC was based on the classification of Salomao *et al.*[23] with the presence of at least 4 of 5 of the following criteria: steatosis (>5%), ballooning, Mallory–Denk bodies, fibrosis, and inflammation. The steatohepatitic component had to involve at least 50% of the total viable tumour surface area. The diagnosis of clear cell HCC was made in tumours with >80% of clear cell morphology from glycogen accumulation.[2] The diagnosis of MTM-HCC was retained in lesions with a macrotrabecular growth pattern in >50% of the tumour.[6]

Statistical analysis

Continuous variables were reported as medians and IQR, after testing with the Shapiro-Wilk normality test. Continuous variables were compared using the ANOVA or Kruskal–Wallis test. Differences in the distribution of categorical variables among the main HCC subtypes were assessed using the Pearson Chi-square test. It should be noted that most tumours in the cohort were NOS-HCC, SH-HCC, or MTM-HCC. Because of the very small number of other subtypes with different histopathological characteristics, our analysis focused on a comparison of these 3 subtypes. Differences in ancillary features favouring benignity were not assessed because of their very low frequency in our cohort. Kaplan–Meier curves were used to compare RFS and OS after resection. Curves were compared using the log-rank test.

Inter-reader agreement was assessed using Cohen's kappa (κ) test with 95% CI for categorical variables and the intraclass correlation coefficient for the continuous variable (size). Numbers and percentages of agreement were provided for categorical variables. Agreement was categorised as poor (<0.00), slight (0.00–0.20), fair (0.21–0.40), moderate (0.41–0.60), substantial (0.61–0.80), or almost perfect (0.81–1.00).

A p value of <0.05 was considered to be statistically significant. Statistical analyses were performed using SPSS software (Version 20.0; IBM Corp., Armonk, NY, USA).

Results

Patients and HCCs

The study cohort included 277 patients (median age 64.0 years [IQR 55.0–70.0 years], with 215 [77.6%] men, median age 64.0 years [IQR 55.0–70.0 years], and 62 [22.4%] women, median age 66.0 years [IQR 57.0–70.0 years]) with 295 HCCs. There were 197 (66.7%) NOS-HCCs, 62 (21.0%) SH-HCCs, 23 (7.8%) MTM-HCCs, and 13 (4.5%) other rare subtypes (including 5 [1.7% of all resected HCCs] clear cell, 4 [1.4%] lymphocyte-rich, 2 [0.7%] scirrhous, and 2 [0.7%] fibrolamellar HCCs). The clinical, laboratory, and histopathological features of patients with NOS-HCC, SH-HCC, and MTM-HCC are reported in Table 1. Features in patients with rare subtypes are provided in Table S1.

HBV infection was more frequently observed in patients with MTM-HCC (52.4% p = 0.004), whereas alcoholic liver disease and non-alcoholic fatty liver disease were more common in patients with SH-HCC (30.5%, p = 0.009; 54.2%, p = 0.001, respectively). Patients with MTM-HCC had significantly higher α-foetoprotein serum levels (median 14,700 ng/ml, p <0.001), higher preoperative hepatic enzymes (aspartate aminotransferase [AST], p <0.001; alanine transaminase [ALT], p = 0.006), and lower albumin (p = 0.023) than patients with other subtypes.

After a median follow-up of 24 months (IQR 10–46 months), the median estimated RFS and OS was 39 months (95% CI 27–51 months) and 88 months (95% CI 70–104 months), respectively.

Table 4. Differences in LI-RADS-defined TIV, LR-M features, and major features in NOS-HCC, SH-HCC, and MTM-HCC subtypes in the entire cohort with contrast-enhanced MRI (n = 227).

Features	NOS-HCC (n = 165)	SH-HCC (n = 48)	MTM-HCC (n = 14)	*p* value	R1 *vs.* R2 N agreement (%) κ value (95% CI)	R1 *vs.* R3 N agreement (%) κ value (95% CI)	R2 *vs.* R3 N agreement (%) κ value (95% CI)
TIV							
R1	7 (4.2)	0 (0)	2 (14.3)	0.052	219 (96.5)	225 (99.1)	219 (96.5)
R2	11 (6.7)	0 (0)	4 (28.6)	**0.001**	0.64 (0.42, 0.87)	0.88 (0.72, 1.00)	0.64 (0.42, 0.87)
R3	7 (4.2)	0 (0)	2 (14.3)	0.052			
LR-M features							
At least 1 LR-M feature							
R1	65 (39.4)	10 (20.8)	6 (42.9)	0.052	177 (78.0)	182 (80.2)	184 (83.7)
R2	66 (40.0)	11 (22.9)	4 (28.6)	0.080	0.52 (0.40, 0.63)	0.55 (0.43, 0.66)	0.57 (0.45, 0.68)
R3	51 (30.9)	11 (22.9)	6 (42.9)	0.314			
At least 1 targetoid feature							
R1	14 (8.5)	3 (6.2)	2 (14.3)	0.630	208 (91.6)	205 (90.3)	208 (91.6)
R2	12 (7.3)	4 (8.3)	0 (0)	0.550	0.41 (0.19, 0.62)	0.39 (0.19, 0.60)	0.44 (0.23, 0.65)
R3	15 (9.1)	4 (8.3)	2 (14.3)	0.788			
Rim APHE							
R1	8 (4.8)	3 (6.2)	2 (14.3)	0.212	214 (94.3)	212 (93.4)	211 (93.0)
R2	6 (3.6)	2 (4.2)	0 (0)	0.750	0.35 (0.08, 0.62)	0.44 (0.21, 0.68)	0.30 (0.05, 0.54)
R3	13 (7.9)	1 (2.1)	2 (14.3)	0.365			
Peripheral 'washout'							
R1	0 (0)	1 (2.1)	0 (0)	0.154	226 (99.6)	223 (98.2)	224 (98.7)
R2	0 (0)	0 (0)	0 (0)	1.000	0.00 (0.000, 0.00)	−0.006 (−0.01, 0.003)	0.00 (0.000, 0.00)
R3	3 (1.8)	0 (0)	0 (0)	0.565			
Delayed central enhancement							
R1	6 (3.6)	0 (0)	0 (0)	0.314	219 (96.5)	222 (97.8)	218 (96.0)
R2	5 (3.0)	1 (2.1)	0 (0)	0.765	0.31 (−0.03, 0.66)	0.53 (0.17, 0.89)	0.16 (−0.15, 0.47)
R3	4 (2.4)	1 (2.1)	0 (0)	0.837			
Targetoid restriction*							
R1	1 (0.6)	1 (2.2)	0 (0)	0.589	215 (99.1)	210 (96.8)	212 (97.7)
R2	1 (0.6)	1 (2.2)	0 (0)	0.079	0.49 (−0.10, 1.00)	−0.01 (−0.02, 0.0003)	0.27 (−0.16, 0.71)
R3	3 (1.9)	2 (4.3)	0 (0)	0.524			
Targetoid appearance on HBP							
R1 (adequate, n = 59)	1 (2.3)	0 (0)	0 (0)	0.828	38 (97.4)	38 (97.4)	39 (100)
R2 (adequate, n = 53)	1 (2.6)	0 (0)	0 (0)	0.818	0.00 (0.000, 0.00)†	0.00 (0.000, 0.00)†	0.00 (0.000, 0.00)†
R3 (adequate, n = 55)	0 (0)	0 (0)	0 (0)	1.000			
Infiltrative appearance							
R1	12 (7.3)	0 (0)	2 (14.3)	0.078	219 (96.5)	219 (96.5)	221 (97.3)
R2	10 (6.1)	0 (0)	2 (14.3)	0.076	0.67 (0.46, 0.88)	0.64 (0.42, 0.87)	0.71 (0.49, 0.83)
R3	10 (6.1)	0 (0)	0 (0)	0.140			
Marked restricted diffusion*							
R1	5 (3.2)	0 (0)	2 (14.3)	0.301	202 (93.1)	201 (92.6)	198 (91.3)
R2	10 (6.4)	0 (0)	2 (14.3)	0.084	0.17 (−0.07, 0.42)	0.19 (−0.03, 0.42)	0.16 (−0.07, 0.40)
R3	11 (7.0)	0 (0)	2 (14.3)	0.085			
Necrosis or severe ischaemia							
R1	45 (27.3)	8 (16.7)	3 (21.4)	0.311	193 (85.0)	196 (86.4)	198 (87.2)
R2	41 (24.8)	8 (14.5)	3 (21.4)	0.490	0.58 (0.46, 0.71)	0.58 (0.45, 0.71)	0.59 (0.46, 0.72)
R3	27 (16.4)	7 (14.6)	3 (21.4)	0.829			
Major features							
Size (mm)							
R1	44.0 (27.0, 64.5)	30.0 (19.0, 46.7)	59.5 (26.0, 100.5)	**0.007**	0.98 (0.97, 0.98)‡	0.98 (0.97, 0.98)‡	0.98 (0.97, 0.98)‡
R2	46.0 (31.0, 70.0)	35.0 (23.2, 54.7)	67.5 (34.0, 130.0)	**0.007**			
R3	44.0 (27.0, 71.5)	30.0 (22.0, 50.2)	61.0 (23.7, 114.7)	**0.011**			
Non-rim APHE							
R1	144 (87.3)	44 (91.7)	11 (78.6)	0.406	202 (89.0)	203 (89.4)	188 (82.9)
R2	153 (92.7)	45 (93.8)	14 (100)	0.572	0.36 (0.51, 0.55)	0.59 (0.45, 0.74)	0.24 (0.08, 0.39)
R3	133 (80.6)	42 (87.5)	10 (71.4)	0.337			
Non-peripheral 'washout'							
R1	145 (87.9)	37 (77.1)	14 (100)	**0.049**	202 (89.0)	198 (87.2)	191 (84.2)
R2	144 (87.3)	39 (81.2)	14 (100)	0.178	0.52 (0.36, 0.68)	0.54 (0.39, 0.68)	0.43 (0.26, 0.57)
R3	131 (79.4)	39 (81.2)	13 (92.9)	0.469			
Enhancing 'capsule'							
R1	117 (70.9)	32 (66.7)	11 (78.6)	0.673	187 (82.4)	185 (81.5)	177 (77.9)
R2	120 (72.7)	30 (65.5)	10 (71.4)	0.391	0.57 (0.46, 0.69)	0.53 (0.41, 0.66)	0.45 (0.23, 0.58)
R3	124 (75.2)	32 (66.7)	12 (85.7)	0.293			

(*continued on next page*)

Table 4 (*continued*)

Features	NOS-HCC (n = 165)	SH-HCC (n = 48)	MTM-HCC (n = 14)	*p* value	R1 *vs.* R2 N agreement (%) κ value (95% CI)	R1 *vs.* R3 N agreement (%) κ value (95% CI)	R2 *vs.* R3 N agreement (%) κ value (95% CI)
Threshold growth							
R1	2 (1.2)	0 (0)	0 (0)	0.684	223 (98.2)	221 (97.3)	221 (97.3)
R2	1 (0.6)	0 (0)	1 (7.1)	**0.032**	−0.008 (−0.01, −0.0001)	0.24 (−0.15, 0.63)	0.24 (−0.15, 0.63)
R3	3 (1.8)	1 (2.1)	2 (14.3)	**0.020**			

Categorical variables are expressed as numbers and percentages in parentheses. The continuous variable (size) is reported as median and IQR (25th to 75th percentiles) in parentheses. Differences between HCC subtypes were assessed using the Pearson $\chi 2$ test for categorical variables. Inter-reader agreement was assessed using the Cohen's kappa (κ) test for categorical variables and intraclass correlation coefficient of the continuous variable (size). Statistically significant values (p <0.05) are highlighted in bold. APHE, arterial phase hyperenhancement; HBP, hepatobiliary phase; LI-RADS, Liver Imaging Reporting and Data System; MRI, magnetic resonance imaging; MTM-HCC, macrotrabecular massive hepatocellular carcinoma; NOS-HCC, not otherwise specified hepatocellular carcinoma; R1, Reader 1; R2, Reader 2; R3, Reader 3; SH-HCC, steatohepatitic hepatocellular carcinoma; TIV, tumour-in-vein.

* Features assessed in 217/227 observations as a result of the lack of diffusion weighted imaging in 10 observations.

† Agreement assessed only in observations considered with adequate HBP for all readers.

‡ Agreement assessed with intraclass correlation coefficient.

RFS and OS curves according to tumour subtypes are provided in Figs S1 and S2.

CT features of NOS-HCC, SH-HCC, and MTM-HCC in the entire cohort

Contrast-enhanced CT was available in the entire cohort in 175 NOS-HCC, 58 SH-HCC, and 20 MTM-HCC. Distribution of TIV, LR-M, and the major features on CT is reported in Table 2. TIV and the presence of at least 1 LR-M feature were more frequently identified in MTM-HCC (p <0.001 for all readers) and (R1, p = 0.001; R2, p = 0.010; R3, p <0.001), respectively. Infiltrative appearance (R1, p = 0.015; R3, p = 0.032) and necrosis or severe ischaemia (R2, p = 0.038, R3, p = 0.004) were observed more frequently in MTM-HCC by 2 of 3 readers (Fig. 2). All 3 readers found size to be significantly larger in MTM-HCCs than in other subtypes (R1, p = 0.002; R2, p = 0.003; R3, p = 0.006). There was no significant difference in the distribution of major imaging features among the 3 main HCC subtypes on CT. Ancillary features favouring malignancy for all HCCs on CT are reported in Table S2. Fat sparing in solid mass was observed by R1, R2, and R3 in 2 (1.1%), 1 (0.6%), and 1 (0.6%) NOS-HCCs; 3 (5.2%), 5 (5.8%), and 3 (5.2%) SH-HCCs; and no MTM-HCCs (R1, p = 0.129; R2, p = 0.002; R3, p = 0.043), respectively, whereas fat in mass (Fig. 3) was depicted in 22 (12.6%), 39 (23.3%), and 14 (8.0%) NOS-HCCs; 19 (32.8%), 19 (32.8%), and 19 (32.8%) SH-HCCs; and 0 (0%), 3 (15.0%), and 1 (5.0%) MTM-HCCs (R1, p <0.001; R2, p = 0.166; R3, p <0.001), respectively.

Inter-reader agreement was substantial for TIV (κ range 0.61–0.74), poor to substantial for LR-M features (κ range −0.01 to 0.68), fair to almost perfect (κ range 0.34–0.97) for major features, slight to moderate for ancillary features favouring malignancy, not HCC in particular (κ range 0.10–0.48), and poor to moderate for ancillary features favouring malignancy, HCC in particular (κ range −0.01 to 0.59).

CT LI-RADS categorisation of NOS-HCC, SH-HCC, and MTM-HCC in high-risk patients

LI-RADS imaging features in the subset of patients considered to be at high risk of HCC are reported in Table S3 (TIV, LR-M, and major features) and Table S4 (ancillary features favouring malignancy). In high-risk patients, TIV, at least 1 LR-M feature, and larger size remained significantly more frequent in MTM-HCC for at least 2 of 3 readers, whereas fat in mass remained more common in SH-HCC by R1 (p = 0.003) and R3 (p = 0.004). LI-RADS categories on CT without and with the association of ancillary features are reported in Table 3. For all readers, LR-5 was categorised less frequently observed in MTM-HCC, although no significant differences were noted when considering all possible categories.

Inter-reader agreement was moderate for LI-RADS categories without (κ range 0.42–0.54) and with (κ range 0.40–0.55) the association of ancillary features.

MRI features of NOS, SH-HCC, and MTM-HCC HCC in the entire cohort

Preoperative contrast-enhanced MRI was available for the entire cohort in 165 NOS-HCC, 48 SH-HCC, and 14 MTM-HCC. Distribution of TIV, LR-M, and major features on MRI is reported in Table 4. TIV was identified significantly more frequently in MTM-HCC by R2 (p = 0.001), whereas it was marginally significant for R1 and R3 (p = 0.052). MTM-HCCs were also found to be larger (R1, p = 0.007; R2, p = 0.007; R3, p = 0.011) and with greater threshold growth (R1, p = 0.684; R2, p = 0.032; R3, p = 0.020) by at least 2 of 3 readers. There was no significant difference in the distribution of other major features among the 3 main HCC subtypes on MRI. Ancillary features favouring malignancy for all HCCs on MRI are reported in Table S5. Fat in mass (Fig. 3) was significantly more common in SH-HCC and was observed by R1, R2, and R3 in 38 (23.6%), 51 (31.5%), and 35 (21.7%) NOS-HCCs; 26 (54.2%), 28 (58.3%), and 26 (54.2%) SH-HCCs; and 2 (14.3%), 7 (50.0%), and 4 (28.6%) MTM-HCCs (R1, p <0.001; R2, p = 0.002; R3, p <0.001), respectively.

Inter-reader agreement was substantial to almost perfect for TIV (κ range 0.64–0.88); poor to substantial for LR-M features (κ range −0.006 to 0.71); poor to almost perfect (κ range −0.008 to 0.98) for major features; slight to substantial for ancillary features favouring malignancy, not HCC in particular (κ range 0.16 −0.68); and poor to substantial for ancillary features favouring malignancy, HCC in particular (κ range −0.008 to 0.70).

MRI LI-RADS categorisation of NOS-HCC, SH-HCC, and MTM-HCC in high-risk patients

LI-RADS imaging features in the subset of patients considered to be at high risk of HCC are reported in Table S6 (TIV, LR-M, and major features) and Table S7 (ancillary features favouring malignancy). In high-risk patients, fat in mass remained more common in SH-HCC and was observed in 12 (48.0%), 13 (52.0%), and 26 (54.2%) SH-HCCs by R1 (p = 0.010), R2 (p = 0.043), and R3 (p = 0.013), respectively. LI-RADS categories on MRI without and with the association of ancillary features are reported in Table 5.

Table 5. LI-RADS categories using major features only and after final adjustment for ancillary features in NOS-HCC, SH-HCC, and MTM-HCC subtypes in high-risk patients with contrast-enhanced MRI (n = 120).

	NOS-HCC (n = 85)	SH-HCC (n = 25)	MTM-HCC (n = 10)	*p* value
LI-RADS categories with major features only				
R1				0.498
LR-3	6 (7.1)	2 (8.0)	0 (0)	
LR-4	9 (10.6)	2 (8.0)	0 (0)	
LR-5	62 (72.9)	20 (80.0)	7 (70.0)	
LR-M	6 (7.1)	1 (4.0)	2 (20.0)	
LR-TIV	2 (2.4)	0 (0)	1 (10.0)	
R2				0.189
LR-3	4 (4.7)	1 (4.0)	0 (0)	
LR-4	5 (5.9)	1 (4.0)	0 (0)	
LR-5	64 (75.3)	22 (88.0)	7 (70.0)	
LR-M	6 (7.1)	1 (4.0)	0 (0)	
LR-TIV	6 (7.1)	0 (0)	3 (30.0)	
R3				0.650
LR-3	5 (5.9)	2 (8.0)	0 (0)	
LR-4	11 (12.9)	4 (16.0)	1 (10.0)	
LR-5	57 (67.1)	18 (72.0)	6 (60.0)	
LR-M	10 (11.8)	1 (4.0)	2 (20.0)	
LR-TIV	2 (2.4)	0 (0)	1 (10.0)	
Agreement	N agreement (%); κ value (95% CI)			
R1 *vs.* R2	98 (81.7); 0.55 (0.40, 0.70)			
R1 *vs.* R3	97 (80.8); 0.59 (0.45, 0.73)			
R2 *vs.* R3	90 (75.0); 0.45 (0.30, 0.60)			
LI-RADS categories with major and ancillary features				
R1				0.498
LR-3	3 (3.5)	1 (4.0)	0 (0)	
LR-4	12 (14.1)	3 (12.0)	0 (0)	
LR-5	62 (72.9)	20 (80.0)	7 (70.0)	
LR-M	6 (7.1)	1 (4.0)	2 (20.0)	
LR-TIV	2 (2.4)	0 (0)	1 (10.0)	
R2				0.165
LR-3	1 (1.2)	0 (0)	0 (0)	
LR-4	9 (10.6)	2 (8.0)	0 (0)	
LR-5	63 (74.1)	22 (88.0)	7 (70.0)	
LR-M	6 (7.1)	1 (4.0)	0 (0)	
LR-TIV	6 (7.1)	0 (0)	3 (30.0)	
R3				0.588
LR-3	3 (3.5)	2 (8.0)	0 (0)	
LR-4	13 (15.3)	4 (16.0)	1 (10.0)	
LR-5	57 (67.1)	18 (72.0)	6 (60.0)	
LR-M	10 (11.8)	1 (4.0)	2 (20.0)	
LR-TIV	2 (2.4)	0 (0)	1 (10.0)	
Agreement	N agreement (%); κ value (95% CI)			
R1 *vs.* R2	95 (79.2); 0.49 (0.34, 0.64)			
R1 *vs.* R3	94 (78.3); 0.53 (0.39, 0.68)			
R2 *vs.* R3	87 (72.5); 0.40 (0.25, 0.55)			

Differences between HCC subtypes were compared using the the Pearson $\chi 2$ test. Inter-reader agreement was assessed using Cohen's kappa (κ) test with 95% CI.
LI-RADS, Liver Imaging Reporting and Data System; MRI, magnetic resonance imaging; MTM-HCC, macrotrabecular massive hepatocellular carcinoma; NOS-HCC, not otherwise specified hepatocellular carcinoma; R1, Reader 1; R2, Reader 2; R3, Reader 3; SH-HCC, steatohepatitic hepatocellular carcinoma; TIV, tumour-in-vein.

Although no significant differences were observed, the frequency of observations categorised as LR-5 in MTM-HCC was lower.

Inter-reader agreement was moderate for LI-RADS categories without (κ range 0.45–0.59) and with (κ range 0.40–0.53) the association of ancillary features.

Other HCC subtypes

The imaging features of other HCC subtypes on CT and MRI are summarised in Table S8. At least 1 LR-M feature was identified in 67–78% of other subtypes on CT and in 50–60% lesions on MRI. There were only 3 and 7 other HCCs in high-risk patients on CT or MRI, respectively. Among them, observations were classified as LR-M or LR-TIV in 66.7% of cases on CT and in 28.6–41.9% on MRI (Table S9).

Discussion

This study evaluated the differences in LI-RADS-defined imaging features and the resulting impact on LI-RADS categorisation of HCC histopathological subtypes in high-risk patients. We observed that the overall distribution of the major features and LI-RADS categories was not different across HCC subtypes. Nevertheless, careful analysis of TIV, LR-M, and ancillary features, as well as clinico-biological data, can be helpful to identity HCC subtypes.

In the present study, MTM-HCCs were found to be significantly larger at diagnosis, but despite histopathological differences among HCC subtypes, no difference was observed in the distribution of the LI-RADS major features (*i.e.* non-rim APHE, non-peripheral 'washout', and enhancing 'capsule') among HCC subtypes on CT and MRI. This was also true in the subset of high-risk patients. These LI-RADS features identify major pathological changes that occur during hepatocarcinogenesis (*i.e.* neoangiogenesis, relative portal blood deprivation, and capsule formation) and that are likely to be comparable among HCC subtypes. This result is highly important and supports the robustness of the LI-RADS classification, whose main goal is high specificity and reproducibility for the non-invasive diagnosis of HCC, regardless of the subtype.

On contrast-enhanced CT, the presence of TIV, at least 1 LR-M feature, infiltrative appearance, and necrosis or severe ischaemia was significantly more frequent in MTM-HCCs than in other subtypes. Similarly, TIV tended to be more frequent in MTM-HCCs on MRI. This is consistent with the histopathological features of tumour aggressiveness in MTM-HCC, including higher Edmonson–Steiner grade, macrovascular invasion, microvascular invasion, and satellite nodules, which is in line with prior investigations.[6,7] Prior studies have assessed the value of various imaging features to differentiate MTM-HCC from non-MTM-HCC on MRI. Mulé *et al.*[12] reported substantial necrosis (defined as necrosis involving at least 20% of the tumour at the largest cross-sectional diameter) as an independent predictive factor of MTM-HCC. Chen *et al.*[13] identified high platelet count, low apparent diffusion coefficient ratio, and necrosis or severe ischaemia as independent predictors of MTM-HCC on gadoxetate disodium MRI. In that study, the sensitivity of necrosis or severe ischaemia was 86% for the diagnosis of MTM-HCC. In our study, necrosis or severe ischaemia was observed on MRI in 21% of MTM-HCCs and was also identified in 16–27% of NOS-HCCs and 14–17% of SH-HCCs, whereas on CT, these features were identified in 40–45% of MTM-HCCs and also in 26–34% of NOS-HCCs and 10–19% of SH-HCCs. This may be as a result of the inconsistent definitions of tumour necrosis in prior studies, fewer MTM-HCCs with available MRI in our cohort, and HCC size differences. Indeed, the extent of tumour necrosis may also be affected by the larger HCC size. In a recent multicentre study, Rhee *et al.*[14] developed 2 diagnostic criteria based on hypovascular components during the hepatic arterial phase to identify MTM-HCC on gadoxetate disodium MRI. However, after scoring, APHE hypovascular components were classified into 11 different patterns, which could be challenging in clinical practice with possible negative effects on inter-reader variability, especially with less experienced readers.[15] In accordance with prior studies,[12,13] we also

observed significantly higher α-foetoprotein serum levels in MTM-HCCs, which was markedly increased in most patients, and a higher rate of hepatitis B infection. Based on our results and available evidence, the preoperative diagnosis of MTM-HCC in clinical practice could be suggested in patients with hepatitis B with large lesions showing TIV or non-targetoid LR-M features and high α-foetoprotein serum levels.

As mentioned above, although the proportion of HCCs classified as LR-5 in patients at high risk decreased in MTM-HCCs for all readers on both CT and MRI, the overall distribution of LI-RADS categories was not statistically different. It is important to emphasise that, according to LI-RADS, the presence of necrosis or severe ischaemia, as well as other non-targetoid features, is not sufficient to categorise an observation as LR-M in the presence of other LR-5 features.[18] Thus, a large subset of HCCs showing non-targetoid features were categorised as LR-5.

Ancillary features provided additional clues for HCC subtyping. On both CT and MRI, fat in mass was significantly more frequent in SH-HCCs than in other subtypes. This was true for the whole cohort as well as for the subset of patients at high-risk of HCC. However, the presence of fat in mass may not be sufficient to reliably predict the SH-HCC subtype, because this feature was also observed in 8–23% and 22–31% of NOS-HCCs as well as 5–15% and 14–50% of MTM-HCCs on CT and MRI, respectively. It is interesting to note that in our study, SH-HCCs were significantly smaller with less frequent TIV. This subtype was associated with a higher grade of steatosis on the background liver parenchyma and a history of non-alcoholic fatty liver disease and alcoholic liver disease, similar to previous pathological studies.[3,24,25] In clinical practice, the preoperative diagnosis of SH-HCC could be suggested in patients with non-alcoholic fatty liver disease or alcoholic liver disease with HCC showing fat in mass without imaging features of TV. Although RFS in SH-HCCs was not significantly lower in the present cohort than in other subtypes, the identification of this subtype could be relevant because it is associated with risk factors of the metabolic syndrome whose prevalence may increase because of the increasing incidence of metabolic syndrome and non-alcoholic fatty liver disease.[26] Further studies are needed to compare the clinical and radiological characteristics of SH-HCC with HCC showing fat in mass.

The main limitation of this single-centre retrospective study is the inclusion of patients with HCC based on surgical resection alone, which could result in a selection bias. In particular, the value of the present results cannot be extrapolated to locally advanced unresectable lesions, metastatic HCCs, or HCCs occurring on a background of decompensated cirrhosis. At present, resection specimens are the gold standard for HCC subtyping because the use of biopsy for accurate HCC subclassification is a matter of debate as a result of known intralesional heterogeneity and possible sampling errors.[8,9] Moreover, the proportion of different subtypes was consistent with that reported in previous Western studies and with the WHO classification.[2,3,12] The assessment of more advanced-stage HCCs, as well as the inclusion of patients with advanced cirrhosis that are not candidates for surgical resection, may have been limited by this approach. Indeed, in our cohort, only 53% of patients met the LI-RADS high-risk population criteria. Moreover, the HCCs in our cohort were large in size, which may have affected the prevalence of LR-M features. Finally, only few patients had available HBP, making it impossible to reliably assess the value of this feature.

In conclusion, the overall distribution of the major features and categories of LI-RADS is not different across HCC histological subtypes. Nevertheless, careful evaluation of TIV, LR-M, and ancillary features, as well as clinico-biological data, can help in the non-invasive diagnosis of HCC subtypes.

Abbreviations

ALT, alanine transaminase; APHE, arterial phase hyperenhancement; AST, aspartate aminotransferase; CT, computed tomography; HBP, hepatobiliary phase; HCC, hepatocellular carcinoma; LI-RADS, Liver Imaging Reporting and Data System; MRI, magnetic resonance imaging; MTM-HCC, macrotrabecular-massive hepatocellular carcinoma; NOS-HCC, not otherwise specified hepatocellular carcinoma; OS, overall survival; RFS, recurrence-free survival; SH-HCC, steatohepatitic hepatocellular carcinoma; TIV, tumour-in-vein; US, ultrasound.

Financial support

The authors received no financial support to produce this manuscript.

Conflict of interest

The authors declare no conflicts of interest that pertain to this work.

Please refer to the accompanying ICMJE disclosure forms for further details.

Authors' contributions

Conceptualisation: MR, VV. Data curation: RC, MDB, RS, AB, LC. Formal analysis: RC, MDB, RS. Methodology: MR, VV, VP. Supervision: MR, VV. Validation: MR, VV, CH, FC, MB. Writing—original draft: RC, MDB, MR. Writing—review and editing: All authors.

Data availability statement

The data that support the findings of this study are available from the corresponding author upon reasonable request.

Supplementary data

Supplementary data to this article can be found online at https://doi.org/10.1016/j.jhepr.2021.100380.

References

[1] Marrero JA, Kulik LM, Sirlin CB, Zhu AX, Finn RS, Abecassis MM, et al. Diagnosis, staging, and management of hepatocellular carcinoma: 2018 practice guidance by the American Association for the Study of Liver Diseases. Hepatology 2018;68:723–750.

[2] WHO Classification of Tumours Editorial Board. WHO Classification of Tumours. 5th edn. Digestive System Tumours. Lyon: IARC; 2019.

[3] Salomao M, Yu WM, Brown Jr RS, Emond JC, Lefkowitch JH. Steatohepatitic hepatocellular carcinoma (SH-HCC): a distinctive histological variant of HCC in hepatitis C virus-related cirrhosis with associated NAFLD/NASH. Am J Surg Pathol 2010;34:1630–1636.

[4] Calderaro J, Couchy G, Imbeaud S, Amaddeo G, Letouzé E, Blanc J-F, et al. Histological subtypes of hepatocellular carcinoma are related to gene mutations and molecular tumour classification. J Hepatol 2017;67:727–738.

[5] Calderaro J, Ziol M, Paradis V, Zucman-Rossi J. Molecular and histological correlations in liver cancer. J Hepatol 2019;71:616–630.

[6] Ziol M, Poté N, Amaddeo G, Laurent A, Nault J-C, Oberti F, et al. Macrotrabecular-massive hepatocellular carcinoma: a distinctive histological subtype with clinical relevance. Hepatology 2018;68:103–112.

[7] Jeon Y, Benedict M, Taddei T, Jain D, Zhang X. Macrotrabecular hepatocellular carcinoma: an aggressive subtype of hepatocellular carcinoma. Am J Surg Pathol 2019;43:943–948.

[8] Calderaro J, Meunier L, Nguyen CT, Boubaya M, Caruso S, Luciani A, et al. ESM1 as a marker of macrotrabecular-massive hepatocellular carcinoma. Clin Cancer Res 2019;25:5859–5865.

[9] Kumar D, Hafez O, Jain D, Zhang X. Can primary hepatocellular carcinoma histomorphology predict extrahepatic metastasis? Hum Pathol 2021:39–46.
[10] Rhee H, An C, Kim H-Y, Yoo JE, Park YN, Kim MJ. Hepatocellular carcinoma with irregular rim-like arterial phase hyperenhancement: more aggressive pathologic features. Liver Cancer 2019;8:24–40.
[11] Vasuri F, Renzulli M, Fittipaldi S, Brocchi S, Clemente A, Cappabianca S, et al. Pathobiological and radiological approach for hepatocellular carcinoma subclassification. Sci Rep 2019;9:14749.
[12] Mulé S, Galletto Pregliasco A, Tenenhaus A, Kharrat R, Amaddeo G, Baranes L, et al. Multiphase liver MRI for identifying the macrotrabecular-massive subtype of hepatocellular carcinoma. Radiology 2020;295:562–571.
[13] Chen J, Xia C, Duan T, Cao L, Jiang H, Liu X, et al. Macrotrabecular-massive hepatocellular carcinoma: imaging identification and prediction based on gadoxetic acid-enhanced magnetic resonance imaging. Eur Radiol 2021:7696–7704.
[14] Rhee H, Cho E-S, Nahm JH, Jang M, Chung YE, Baek S-E, et al. Gadoxetic acid-enhanced MRI of macrotrabecular-massive hepatocellular carcinoma and its prognostic implications. J Hepatol 2021;74:109–121.
[15] Feng Z, Li H, Zhao H, Jiang Y, Liu Q, Chen Q, et al. Preoperative CT for characterization of aggressive macrotrabecular-massive subtype and vessels that encapsulate tumor clusters pattern in hepatocellular carcinoma. Radiology 2021;300:219–229.
[16] Zhu Y, Weng S, Li Y, Yan C, Ye R, Wen L, et al. A radiomics nomogram based on contrast-enhanced MRI for preoperative prediction of macrotrabecular-massive hepatocellular carcinoma. Abdom Radiol (Ny) 2021;46:3139–3148.
[17] Inui S, Kondo H, Tanahashi Y, Fukukura Y, Sano K, Morisaka H, et al. Steatohepatitic hepatocellular carcinoma: imaging findings with clinicopathological correlation. Clin Radiol 2021;76:160.e15–160.e25.
[18] American College of Radiology. CT/MRI liver imaging reporting and data system v2018 core. https://www.acr.org/Clinical-Resources/Reporting-and-Data-Systems/LI-RADS/CT-MRI-LI-RADS-v2018. Accessed July 12 2021.
[19] An C, Park S, Chung YE, Kim D-Y, Kim S-S, Kim M-J, et al. Curative resection of single primary hepatic malignancy: liver Imaging Reporting and Data System Category LR-M portends a worse prognosis. AJR Am J Roentgenol 2017;209:576–583.
[20] Choi SH, Lee SS, Park SH, Kim KM, Yu E, Park Y, et al. LI-RADS classification and prognosis of primary liver cancers at gadoxetic acid-enhanced MRI. Radiology 2019;290:388–397.
[21] Brunt E, Aishima S, Clavien P-A, Fowler K, Goodman Z, Gores G, et al. cHCC-CCA: consensus terminology for primary liver carcinomas with both hepatocytic and cholangiocytic differentiation. Hepatology 2018;68:113–126.
[22] Kambadakone AR, Fung A, Gupta RT, Hope TA, Fowler KJ, Lyshchik A, et al. LI-RADS technical requirements for CT, MRI, and contrast-enhanced ultrasound. Abdom Radiol (Ny) 2018;43:56–74.
[23] Salomao M, Remotti H, Vaughan R, Siegel AB, Lefkowitch JH, Moreira RK. The steatohepatitic variant of hepatocellular carcinoma and its association with underlying steatohepatitis. Hum Pathol 2012;43:737–746.
[24] Shibahara J, Ando S, Sakamoto Y, Kokudo N, Fukayama M. Hepatocellular carcinoma with steatohepatitic features: a clinicopathological study of Japanese patients. Histopathology 2014;64:951–962.
[25] Taniai M, Hashimoto E, Tobari M, Kodama K, Tokushige K, Yamamoto M, et al. Clinicopathological investigation of steatohepatitic hepatocellular carcinoma: a multicenter study using immunohistochemical analysis of adenoma-related markers. Hepatol Res 2018;48:947–955.
[26] Low HM, Choi JY, Tan CH. Pathological variants of hepatocellular carcinoma on MRI: emphasis on histopathologic correlation. Abdom Radiol (Ny) 2019;44:493–508.